IEEE Access
Multidisciplinary | Rapid Review | Open Access Journal

Received 10 May 2024, accepted 21 May 2024, date of publication 28 May 2024, date of current version 6 June 2024.

Digital Object Identifier 10.1109/ACCESS.2024.3406936

RESEARCH ARTICLE

Dual Frequency Multi-Functional via-Less Leaky Wave Antenna Featuring Enhanced Frequency Sensitivity and Dual Beam Scanning Capability

BASUDEV MAJUMDER[1], (Member, IEEE), SARATH SANKAR VINNAKOTA[2], MADHUSUDHAN GOUD RANGULA[3], (Member, IEEE), AND KRISHNAMOORTHY KANDASAMY[3], (Senior Member, IEEE)

[1]Microwave Electronics Division, Department of Avionics, Indian Institute of Space Science and Technology (IIST), Department of Space, Government of India, Thiruvananthapuram 695547, India
[2]Department of Electrical and Electronics Engineering, Birla Institute of Technology and Science, Pilani (BITS Pilani), Hyderabad Campus, Hyderabad, Telangana 500078, India
[3]Department of Electronics and Communication Engineering, NITK Surathkal, Surathkal, Karnataka 575025, India

Corresponding author: Basudev Majumder (bmbasudev30@gmail.com)

This work was supported in part by the Science and Engineering Research Board (SERB), Government of India, under the Core Research Grant CRG/2023/004269.

ABSTRACT In this paper we present a dual band low cross-polarized periodic microstrip leaky wave antenna (LWA) based on the multi mode resonator concept (MMR). The structure is capable of frequency dependent backward dual-beam steering and fast forward beam scanning in the upper and lower operating band, respectively. A gap loaded microstrip line is used as a host transmission line to feed the combination of the periodic patch radiators on the top and the bottom etched slots leading to the generation of the forward and the backward space harmonics. The etched ring slots at the bottom surface of the structure are not only responsible for steering the beam in the backward direction in the bottom hemisphere in its upper band but also adds radiation diversity in the overall radiation mechanism in its two operating bands. The potential use of this antenna resides in its ability to produce in-plane fast forward beam steering suitable for autonomous vehicle navigation systems in its lower band and out-of-plane backward-symmetric dual beam steering in the upper operating bands, suitable for tracking in relay systems.

INDEX TERMS Dual band, leaky wave antenna (LWA), dispersion, beam scanning rate, radiation discontinuity, microstrip.

I. INTRODUCTION

Leaky Wave Antennas are very popular for wireless and radar systems applications due to their frequency-dependent beam scanning, high gain, low cost, simple feed and narrow beamwidth properties [1]. They are generally classified by their radiation mechanism such as periodic, uniform and quasi uniform. Periodic LWAs are capable of giving backward space harmonics while the quasi uniform LWAs can only generate forward radiation. LWAs have been realized in various types of transmission line such as micrsotrip, waveguide, Substrate Integrated Waveguide (SIW) and Surface Plasmon Polariton (SPP). Since its discovery, the majority of the investigations deal with defining new techniques to suppress the open stop band to get backward to forward beam scanning. Some of these are based on introducing complimentary open circuited microstrip-stub [2], using Multi Mode resonator (MMR) [3], [4], CRLH like based guiding structure [5], creating transverse and longitudinal asymmetry in the traveling wave structure [6]. Other attractive features of LWA such as multi-band, dual-beam and fast scanning have been explored of late. Dual-band or multi-band LWAs have been proven to be compact since different frequency bands can share same volume of

The associate editor coordinating the review of this manuscript and approving it for publication was Ladislau Matekovits.

the antenna, thereby reducing the size. Several multi-band leaky wave antennas have been designed with the following key mechanism such as microstrip line fed slot arrays with different profile modulations [7], combining transverse slot and slow wave structures together on SIW [8], capacitive slot (such as 'U') on Half Mode Substrate Integrated Waveguide (HMSIW) structure [9], [10], back to back slotted SIW [11], Dual Mode Composite based microstrip line (DMC-MSL) [12], and via loaded stepped impedance resonator (SIR) like structure [13]. These antennas only posses forward and backward beam scanning capability in their two operating bands but except [13], among all others' dual beam behaviour is omitted. LWAs with symmetrical/asymmetrical beam scanning capability, in either in-plane or out of plane are useful in transmitting the received signal to/from any surrounding objects. This kind of antenna find its usefulness in the relay stations as can be seen from the Fig. 1. Dual beam scanning antennas mounted on relay stations (MHRS, RS, BS) can receive the signal from a particular angular direction and redirect the signal where the principle beam cannot be reached in the same frequency band and thereby increasing the coverage range. In addition to that, the dual beam antennas supporting any additional beam like shown in the red color arrows in Fig. 1, can further be engaged in independent communication. Dual beam leaky wave antennas having out of plane radiation pattern have been reported earlier either to enhance the scan range or to setup concurrent communication from two different direction. These antennas are generally realized based on the periodic perturbation of the mirrored or non-mirrored slot-radiator etched from the top and/or the bottom surface of the guided structure [4], [5], [14], [15], [16], [17]. Leaky Wave Antennas having in-plane dual-beam scanning are commonly realized by exciting multiple modes. Such as based on the higher order modes of the microstrip line [18] or combining two or three different unit cells in one period [13], [19]. The antennas reported in [5], [14], [15], [16], [17], [18], and [19] support only single band of operation. In references [13] and [20] authors have reported dual band and triple band leaky wave antennas, respectively, which support in plane dual beam scanning in one of its operating bands by combining two different leaky wave resonators. However, all these aforementioned antennas do not possess the key feature of faster scanning rate. The radiation discontinuity presented in those antennas do not support larger coverage with smaller frequency range. Generally LWAs implemented using SIWs or HMSIWs suffer from low scanning rate and higher cross polarization level as can be seen from some of the earlier and some of the fundamental work like [9], [13], and [21]. However, authors in reference [21] has designed a SIW based quasi-uniform type LWA with very small period and a larger slot length to improve the scanning rate based on the higher slope of the reactance in their proposed radiation discontinuity, but that operates in single frequency band (30-34 GHz) and can scan only in the forward direction. Additionally, the fabrication of SIW/HMSIW based guided structure brings more complexity

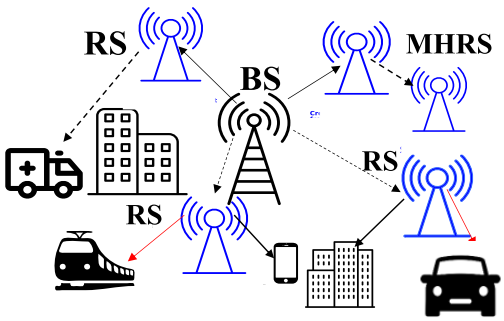

FIGURE 1. Dual beam antenna in relay station [BS: Base station, RS: Relay station, MHRS: Multi hop relay station, Black arrow stands for dual beam].

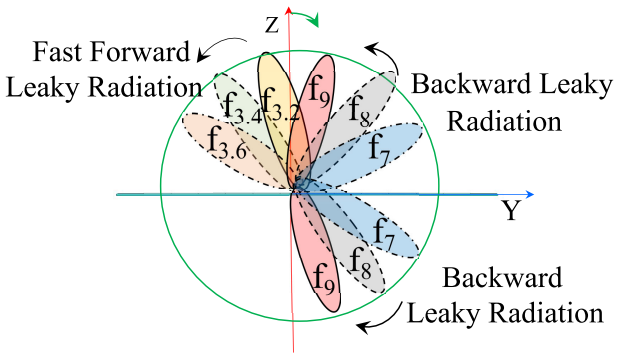

FIGURE 2. Conceptual illustration of the proposed leaky wave antenna along with its pattern.

and challenges due to the presence of series of vias or iris. Nevertheless, SIWs and HMSIWs are very common in literature to design leaky wave antennas because the shunt inductance provided by the vias can easily be controlled to change the characteristic of the complex propagation constant as desired. In the recent past, Leaky wave antennas with faster beam scanning capability have gained much attention due to its fast scanning capability within the smaller frequency range, thereby reducing the effort of the Analog-to-Digital converters of the front end systems. This ensures faster scanning coverage, economizes the spectrum usage and helps in realizing the fast tracking in radar systems [22], [23], [24], motion detection systems [25], automotive cruise control and forward collision alert radar sensor [26]. In the recent years, different novel radiation discontinuities are investigated to realize the faster beam scanning rate LWA with additional improved features. Like in reference [27] authors have created a stop-band deliberately close to the cutoff of a leaky mode leading to the sharpening of the phase constant and thereby exhibiting a strong dispersion. In reference [28] also, forward scanned single band LWA with faster beam scanning capability is proposed based on microstrip based compli-mentary slot stub technique. The complimentary arrangement engineers the group delay across the period and thereby leading to the enhancement of the slope of the dispersion curve. Reference [29] uses capacitively coupled via loaded meandered line as the primary radiation discontinuity to

achieve high scanning rate LWA with broadside radiation. In reference [30] Spoof surface plasmon polariton (SPP) structures are integrated with HMSIW (HMSIW-SPP) to modify the effective dielectric constant to achieve dual beam leaky wave antenna with high scanning rate without any broadside radiation. In [31] and [32] higher order space harmonics are utilized to design the fast scanned leaky wave antenna in the forward direction. Designing high scanning rate and radiation efficient planar LWAs with additional features such as multi band, dual-beam, simple feed, stable gain and low cross polarization are still a challenging task and are very rarely found in the literature.

In this paper, a microstrip based dual frequency via-less leaky wave antenna with fast forward and dual backward beam scanning feature is proposed. The gap loaded microstrip line in the middle layer, together with the top periodic patches excite the resonant ring slots etched at the ground plane. The radiation mechanism of the unit cell helps achieving the simultaneous dual beam scanning by combining the leaky radiation in the upper hemisphere from the patches at top and an aperture radiation in the bottom hemisphere from the etched rectangular slots. In addition to that, the proposed antenna provides a faster scanning rate at the lower operating band. A graphical illustration of the radiation pattern and its scanning has been depicted in Fig. 2. The proposed leaky wave antenna is designed and numerically verified in CST MWS. Its performance is measured and compared with the obtained simulated results. The resulting leaky-wave antenna can scan in forward direction from 12^0 to 57^0 with the scanning rate of 112.5^0/ GHz at lower band (3.2 GHz - 3.6 GHz) (frequency sensitivity of 0.1125^0/MHz) and can produce two simultaneous out of plane backward scanning beam from -42^0 to -2^0 and -135^0 to -178^0 at the upper band (6.9 GHz - 9.1 GHz) which can be used to set up communication and in two different direction concurrently. The proposed antenna is only $5.6\lambda_0$ long (at 6 GHz) and features simpler implementation and easier fabrication with stable far-field radiation properties.

II. ANALYSIS OF THE RADIATION DISCONTINUITY AND ITS EFFECT ON THE LEAKY MODES

A. DISPERSION ANALYSIS AND THE RADIATION MECHANISM OF THE PROPOSED UNIT CELL

In this section, the unit cell of the proposed leaky wave antenna is numerically characterized to get the physical insight about the working principle of the overall antenna. The unit cells for leaky wave antennas act as the primary radiating discontinuities which also determines the complex propagation constants of the related leaky modes. In this section its behavior is fully studied to understand the leakage mechanism and the associated phase constant of it. The unit cell of the proposed antenna consists of two layers as can be seen from Fig. 3(a)-(d). The top patch is printed on a 0.5 mm thick dielectric with $\epsilon_{r1} = 3.38$. The gap loaded transmission line is just underneath the top patch and printed on a dielectric

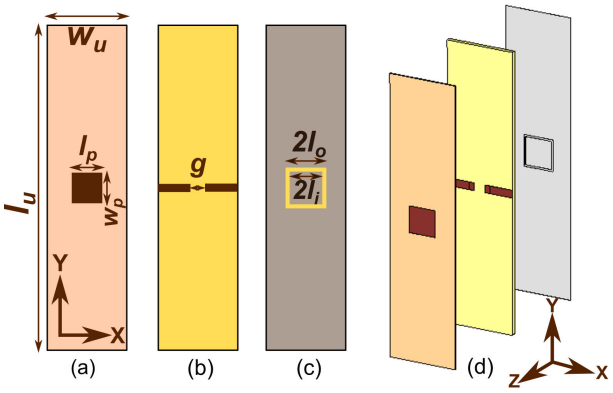

FIGURE 3. Geometry of the unit cell (a) Top layer (b) Middle layer (c) Bottom layer; (d) Exploded view of unit cells; dimensions (in mm): dimensions (in mm): ($l_u = 60$, $w_u = 20$, $l_p = 8$, $w_p = 6.4$, $l_o = 5$, $l_i = 4.5$, $g = 5.4$).

with $\epsilon_{r2} = 2.2$ and thickness (d) of 1.27 mm. The bottom slab thickness and permittivity is chosen as per the equation [1], [33]

$$N < \frac{k_0 d}{\pi}\sqrt{\epsilon_{r2} - 1} \tag{1}$$

where $k_0 = \omega\sqrt{\mu_0\epsilon_0}$ to ensure the excitation of only TM_{01} surface wave mode. The condition N<1 corresponds to single-mode (fundamental mode) propagation. A centrally symmetric ring slot of 0.5 mm width has been etched from the ground of the bottom layer. This TM_{01} surface wave mode periodically perturbs the top patch and the bottom ring slot underneath combinedly. The modal behaviour of this unit cell with and without the bottom slot is obtained in Fig. 4(a) by numerically solving the Bloch-Floquet theorem at the input and output terminals of the unit cell. The dotted blue line shows the air line. The electromagnetic wave becomes leaky when $\beta/k_0 < 1$. The proposed unit cell exhibits two leaky regions(corresponding to the leaky mode β_1) which are marked as a shaded region. The lower band ranges between 3.2 GHz and 3.6 GHz, and the upper band ranges between 6.7 GHz and 9 GHz. The non radiating mode exists in between the lower and upper bands. In the lower band ($\beta > 0$) the radiation occurs in forward direction and in the upper band ($\beta < 0$) the antenna radiates in a backward direction. The modal distribution of the first two leaky modes (β_2) of the grounded unit cell is also included for comparison in Fig. 4(a). Fig. 4(b) studies the impact of the proposed radiation discontinuity on the host open ended gap loaded microstrip lines in step by step manner. It can be seen that in the absence of the patch and the slot discontinuity, the open-ended microstrip line (OMSL) produces two resonances one at 5.6 GHz and another at 10 GHz. The loading of the patch or ring slot separately, brings an additional shunt (parallel RLC) resonance at 7.6 GHz or 5.6 GHz, respectively. This is clear from the black solid curve (patch + OMSL) and blue dotted curve (OMSL+slot) in the same figure. These newly created shunt resonances are due to the effect of the

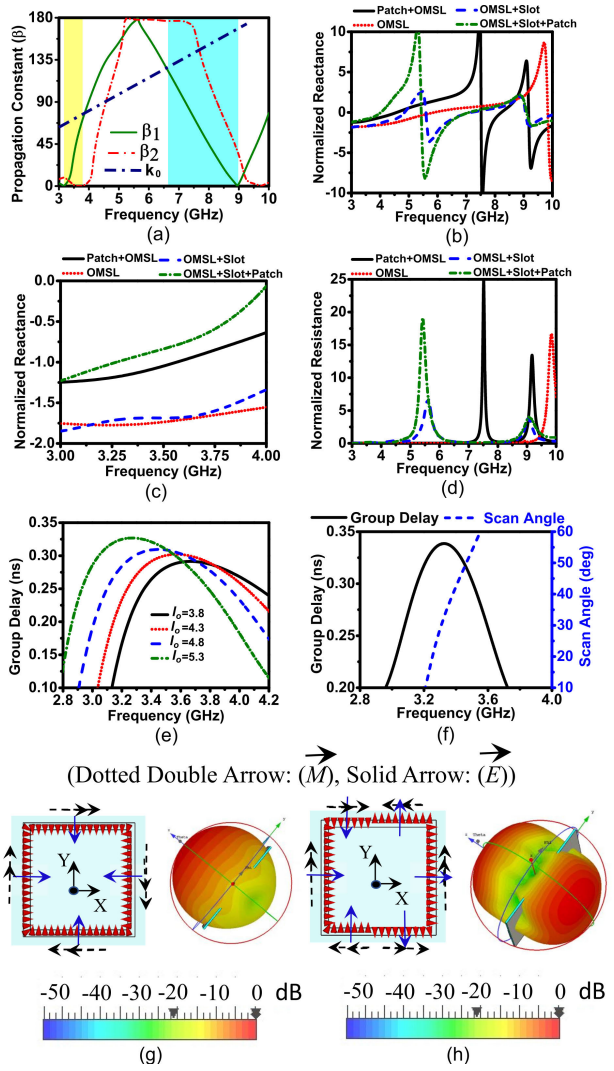

FIGURE 4. **(a) Dispersion diagram: β_1 - with ring slot, β_2 - without ring slot (b) Normalized input reactance with frequency (c) Normalized input reactance zoomed at lower frequency band (d) Normalized input resistance with frequency (e) Group delay variation l_o (f) Group delay and scan angle variation with Frequency; E-field and radiation pattern (g) 2.99 GHz (h) 5.99 GHz [Horizontal color ramp shows the radiated power variation].**

a Multi Mode Resonator (MMR) in operation. The loading of this, shifts the original OMSL shunt resonance slightly at the lower side at around 9 GHz. In both these cases, an additional series resonance could be observed at 8.5 GHz and 7.5 GHz for patch and slot loading, respectively, between each of their individual shunt resonances. The occurrence of the series resonance is mainly due to the complimentary reactance properties between these two series connected parallel RLC resonator in the frequency band of our interest. The inductive contribution due to the patch or the slot cancels the capacitive effect of the OMSL in terms of their reactance at particular frequency point thereby satisfying the series resonator condition of the whole RLC resonator tank. It is evident from both the Fig. 4(a) and (b) that the shunt resonance provided by the ring slot widens the frequency zone of interest with stable radiation as compared the case when patch alone exists. The patch alone can produce a strong shunt resonance with high slope of reactance particularly at the lower band as compared to the ring slot but the frequency band of interest around its series resonance is observed less. In order to claim their individual benefits, both the radiation discontinuities (the patch and the slot) are combined and loaded on the OMSL. This can be observed from the green dotted curve (OMSL+slot+patch) of normalized reactance in the same figure. Although, the dimension of the patch can be tuned to widen the frequency band of interest and provide sufficient high reactive loading at the lower band, but it could not produce any additional beams at the bottom hemisphere. The combined reactive loading of the patch and slot makes the first shunt resonance of the ring slot stronger and provides a higher slope of reactance at the lower band with almost having minimal impact on the upper shunt resonance due to OMSL at 9 GHz. The leads to the increased slope in the input reactance and can be clearly seen from the Fig. 4(b) as well as from Fig. 4(c). In addition to this, the combined effect provides the wider frequency band of interest around the series resonance at 7.5 GHz. The two shunt resonator mode can be flexibly controlled by changing the geometrical parametrs of the unit cells. These modes have been optimized in such a way so that real part of the normalized impedance around 7.5 GHz and 3.2 GHz can provide sufficiently small and stable value for stable radiation pattern and good beamwidth across the entire frequency of interest of the LWA. This can be seen from the real part of the input impedance curve given in Fig. 4(d). Being it a leaky wave antenna, the wave should be slowly attenuated travelling wave to contribute to the leaky radiation. These frequencies should be away from the resonance points where the real part of the input impedance is very high and the imaginary part undergoes a fast change such as 5.5 GHz and 9 GHz, the shunt resonances. For the proposed structure since the real part of the input impedance is very low at 3.2 GHz and 7.5 GHz, the wave is slowly attenuated and hence our frequency of interest. These resonances and their operating mechanism have been further understood with the help of an approximate circuit model, later in this section. When the real part of input impedance is very high and the imaginary part undergoes a sharp change as already pointed out, such as 9 GHz and 5.5 GHz (shunt resonance) for our proposed structure, the energy is cut off and the antenna will not leak any travelling wave. That is why around 9 GHz although the next forward mode starts, but it can only radiate when it can be made to operate away further its resonance. Additionally, controlling the shunt resonances provided by the combined effect of the patch and the slot not only allows to have compact foot print but also leads to the higher slope in the reactance profile and hence in the group delay. Engineering the group delay can have a positive impact in order to obtain fast scanning feature. This fact has been understood further, using the equations below. The scan angle is θ and ω is the angular frequency. The scan angle can also

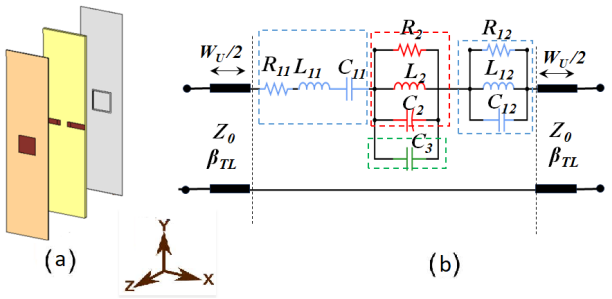

FIGURE 5. (a) Exploded view of the unit cell (b) Equivalent circuit model.

be expressed by

$$\theta(\omega) = \sin^{-1}\left[\frac{\beta(\omega)}{k_0}\right] = \sin^{-1}\left[\frac{c\beta(\omega)}{\omega}\right] \tag{2}$$

c is the speed of light in air. Putting this expression of $\theta(\omega)$ into the scanning rate expression $\varrho(\omega_0)$, it can be shown that

$$\varrho\,(\omega_0) = \frac{1}{\omega_0 \cos\theta\,(\omega_0)}\left[c\frac{d\beta}{d\omega} - \sin\theta\,(\omega_0)\right] \propto d\beta/d\omega \tag{3}$$

The scanning rate, ϱ around a specific frequency, ω_0, is defined by

$$\varrho\,(\omega_0) = \left.\frac{d\theta(\omega)}{d\omega}\right|_{\omega=\omega_0} \tag{4}$$

From this equation it can be understood that to obtain a high scanning rate, it is required to have a periodic unit cell with highly dispersive guiding structure. This indicates to the larger group delay across the period of the unit cell of the leaky wave antenna. The simulated group delay response are calculated and shown in Fig. 4(e) for different value of the ring slot width. It is noted that for a fixed gap between the open ended microstrip line and the fixed size of the patches located at the top layer, the group delay parameter can be controlled by controlling the size of the ring slot. The simulated peak group delay shifts at the lower side as the half width of the resonant slot l_o varies between 3.8 mm and 5.3 mm. The width of the ring slot has minimal impact in all these parameter. It is worth pointing out that the highly dispersive forward branch offers a larger group delay in the lower band resulting in a faster scanning rate. Fig. 4(f) reports the group delay profile with the half width ring slot of 5 mm with other optimized parameters like gap (g) and the patch dimensions. Corresponding to this, the scan angle is also shown in the same figure. From this, it can be inferred that the forward branch can provide frequency sensitivity up-to 0.1125^0/MHz while scanning at the lower band between 3.2 GHz and 3.6 GHz. Fig. 4(g) and (h) studies the unit cells' resonance performance in terms of its' electric field distribution and the corresponding radiation pattern at 2.99 GHz and 5.98 GHz, respectively by terminating it with suitable boundary conditions. It can be seen that 2.99 GHz the bottom ring slot is not resonating and the resultant fields in both the horizontal and vertical arms of the ring, being out of phase cancel each other. As a result, the structure leaks very less power (-20 dB down) in the bottom half plane as compared to its broadside. On the contrary, at 5.98 GHz the circumference of the slot being comparable with the operating wavelength, it becomes resonant and the aperture electric fields on the two vertical arms of the ring slot, being in phase, add up in the far-field producing a strong radiation at the lower hemisphere. The electric fields from the transverse slots (horizontal arm) cancel in both the principal planes, leading to very low cross polarization in its two operating bands. The aforementioned analysis justifies the fact that the proposed antenna can exhibit two different unit radiation pattern at two different frequency points namely 2.99 GHz and 5.99 GHz. In the lower resonating frequency it produces a unidirectional pattern while at 5.99 GHz it produces a bi-directional unit pattern. Moreover, the period of the antenna being at 20 mm, ensures no occurrence of grating lobes in its radiation pattern. The perfect horizontal electric field (X-Polarized) distribution in the antenna unit cell resonator ensures no occurrence of grating lobes in the elevation plane. Fig. 5(b) shows an equivalent and approximate circuit model of the proposed unit cell. The impedance behavior as reported in 4(b)-(d) has been utilized to extract this circuit model. From the detailed analysis given in Fig. 4(b) to 4(d) it can be seen that the microstrip line based OMSL produces series resonance near 5.6 GHz where the imaginary part of the input impedance is zero and a shunt resonance at 10 GHz where the imaginary part input impedance undergoes sharp jump. This two resonances at 5.6 GHz and 10 GHz have been modeled using a series connected series RLC circuit (consists of R_{11}, L_{11}, C_{11}) and a parallel RLC circuit (consists of R_{12}, L_{12}, C_{12}), respectively. When the patch is loaded on top of it, the shunt resonance mentioned above shifts slightly towards left at 9 GHz and in addition to that one more extra shunt resonance is created at 7.6 GHz due to the patch which was shown by a parallel RLC resonance circuit (consists of R_2, L_2, C_2). These two series connected parallel RLC branches create an additional series resonance at 8.5 GHz where the imaginary part of the input impedance is zero. The loading of the patch also shifts the OMSL series resonance at 4.4 GHz. Further the loading of the rectangular slot at the ground creates capacitive loading on the patch resonance, leading to the shift of the patch shunt resonance at 5.6 GHz from 7.6 GHz. The position of the series resonance between the shunt OMSL resonance (9 GHz) and the combined patch slot shunt resonance (5.6 GHz) now becomes 7.1 GHz. In addition to that the bandwidth around this frequency also increases as compared to the only patch loading. The position of the shunt resonance at 9 GHz remains intact due to the loading of the rectangular slot. The position of the first series resonance becomes 4.1 GHz. So the loading of the rectangular slot is equivalently presented by the capacitance C_3 which is seen to be connected in parallel with the R_2, L_2, C_2. So, overall these three resonators create two shunt resonances and two series resonances between 3 GHz and 10 GHz, which is

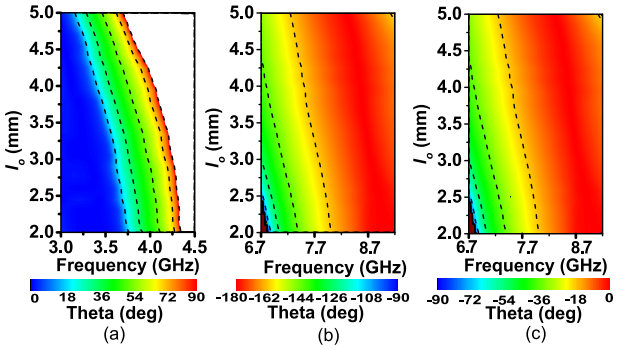

FIGURE 6. Theoretical scan angle variation over frequency and outer ring slot (a) Lower band (b) Upper band lower hemisphere (Beam 1) (c) Upper band upper hemisphere (Beam 2).

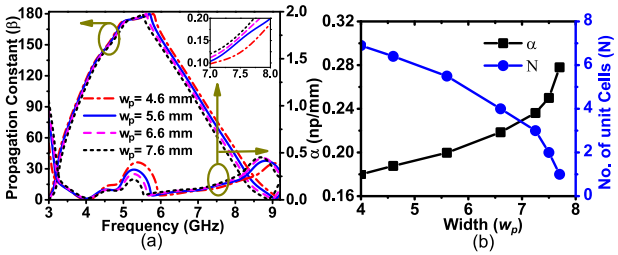

FIGURE 7. (a) Dispersion behavior over frequency with change in patch width (w_P) (b) Leakage constant and no. of unit cells with change in patch width (w_P) at 8 GHz.

our frequency band of interest. The approximate equivalent circuit model can be seen in Fig. 5(b) and the corresponding layer of stack at Fig. 5(a). Both the lower and the upper band the polarization is horizontal in nature and the fringing fields from the vertical arm of the patch edge creates this radiation. The model description given here is highly approximate in nature and not unique. Even though the model is not extracted from the principles of electromagnetic point of view, still it helps in understanding the resonances, operating mechanism and the radiation principle of the proposed antenna.

The presence of the leaky resonator allows the antenna to generate dual beam at the upper band. The unit radiation pattern is modulated with the extracted frequency dependent phase constant value as depicted in β_1 of Fig. 4(a) and produce the fast forward and simultaneous dual backward beam in the respective leaky wave band of interest. This fact has been further understood by the traditional pattern multiplication and phased array antenna theory [33]. In this method, the main beam directions of element pattern and array factor are defined as θ_{me} and θ_{ma}, The θ_{ma} depends on the frequency due to its frequency dependent dispersive behavior. Modified pattern multiplication can be written as:

$$F\left(\theta, \theta_m, f\right) = F_l(\theta, \theta_{me}) \times F_a\left(\theta, \theta_{ma}(f)\right). \tag{5}$$

Due to the its diverse unit pattern in the lower band and the upper band, the function $F_l(\theta, \theta_{me})$ changes and hence the group pattern $F(\theta, \theta_{m,f})$. The bidirectional behavior of the element pattern at the upper band leads to the backward dual beam scanning while directional unit pattern in the lower band leads to forward direction scanning. The relation between the array factor and phase constant is given as:

$$F_a\left(\theta, \theta_{\mathrm{ma}}(f)\right) = A_0 + A_1 e^{j\cdot\psi(f)} + A_2 e^{j2\cdot\psi(f)} + \cdots + A_n e^{jm\cdot\psi(f)}, m = 0, 1, \ldots, N-1 \tag{6}$$

$$\psi(f) = k_0 \Delta d \sin\theta + \delta(f) \tag{7}$$

$$\delta(f) = \beta(f)\Delta d \tag{8}$$

In the above equations, A_n is the excitation amplitude of the nth element, δf is the phase difference between the $(n-1)^{th}$ and n^{th} elements, which can be changed with frequency. The constants N, Δd and k_0 are the number of elements and the element spacing (i.e.$\Delta d = W_u$), and the wave-number in free space, respectively. Thus, the phase constant δf directly can determine the array factor $F_a\left(\theta, \theta_{ma}(f)\right)$.

Fig. 6 reports the variation of the calculated scan angle with frequencies for different dimensions of the ring slots. Fig. 6(a) demonstrates that, in the lower operating band a steep variation of around 90^0 can be observed as the half length of the ring slot is increased 2 mm to 5 mm with increasing frequency. Fig. 6(c) shows the scan angle variation in the upper band at the upper hemisphere (named as Beam 2). The presence of the ring slot at the bottom produces another symmetric backward beam and scans in the bottom hemisphere (named as Beam 1) in the same operating band. This is shown in Fig. 6(b). From these plots, it can be inferred that the leaky ring resonator produces dual beam and due to which the antenna scans bidirectionally in the backward direction in the upper band.Fig. 7 represents the variation of the modal behavior of the unit cell with the width (w_p) of the top patch. It can be noted that, as the width increases, the variation in the propagation constant β remains negligible. The leakage loss α in the lower operating band is also observed negligible as well. However, at the upper operating band the leakage increases as the width of the patch increases (as shown in inset of Fig. 7(a)). This fact has been further verified by the Fig. 7(b). Different widths of the top patch have been utilized in our proposed leaky wave antenna to control the illumination of the radiating aperture at the upper operating band. The arrangement of the different patches based on its sizes is selected as per the value of N shown in Fig. 7(b). Since the structure is symmetric with respect to its centre only, half the portion is considered. A tapered illumination profile of the leakage loss ensures reduced side lobe level having negligible change in the beam pointing angle [33].

B. THEORY OF CHARACTERISTIC MODE (TCM) ANALYSIS OF THE PROPOSED UNIT CELL

The unit cells have been connected in cascade to construct the whole leaky wave antenna along with the suitable feed. Fig. 8 (a) -(b) compares the typical radiation pattern of the grounded and the ungrounded (proposed) leaky wave antenna at the upper operating band. The grounded leaky wave antenna does

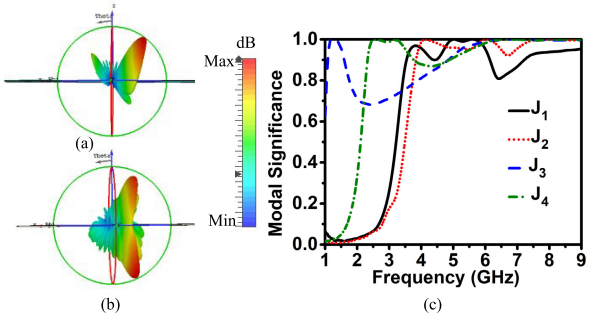

FIGURE 8. (a) Radiation pattern of grounded and ungrounded Leaky Wave Antenna and Modal Significance curve (a) Grounded Leaky Wave Antenna at 7.5 GHz (b) Ungrounded Leaky Wave Antenna at 7.5 GHz (c) Modal Significance of the Unit cell for first four modes.

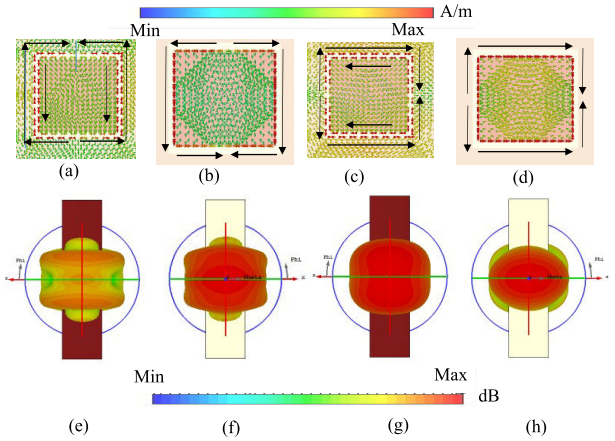

FIGURE 9. Surface Current distribution and Far field behavior for first two modes (a) J1, Bottom, (b) J1, Top (c) J2, Bottom (d) J2 top; Radiation Pattern (e) J1, Bottom, (f) J1, Top (g) J2, Bottom, (h) (d) J2 top.

not contain the ring slot at the bottom. The radiation from it, is observed to be unidirectional as can be seen from the Fig. 8(a), while the ungrounded one radiates bidirectionally both in the upper and the bottom hemisphere. This can be shown from the Fig. 8(b). Both these antennas are found to be radiated and scanned in the backward direction as per their dispersive behavior predicted in the Fig. 4 (a). In order to have a better physical insight about the bottom radiation from the ungrounded one and to understand the fact that it is due to the presence of the resonant leaky ring slot, all the real modes inside the unit cell structure is studied, independent of any excitation using the Theory of Characteristic Modes (TCM) analysis [34] with the help of the multi layer solver in the CST MWS. They are depicted in the Fig. 8(c) and Fig. 9. Fig. 8(c) represents the modal significance of the first four modes of the proposed unit cell. The modes having modal significance value of more than 70 percent are potentially responsible to produce the resonance and radiate efficiently. Modal significance (MS) presents the normalized current amplitude with a range from 0 to 1 and can be calculated as

$$\mathrm{MS} = \left| \frac{1}{1 + \lambda_n} \right| \tag{9}$$

At the resonance $\lambda_n = 0$ the corresponding mode has MS value of 1. Fig. 9 (a)-(h) show the modal surface current distribution and the far-field behavior of the proposed unit cell for the first two modes. From these figures, it can be interpreted that the proposed unit cell can produce bi-directional radiation of both polarization if it is excited suitably. The excitation of the modal surface currents control the far field radiation behavior. In the present design philosophy, the X-directed open ended microstrip lines excite the ring slots with modal surface current distribution along the X direction (Fig. 9 (c) and Fig. 9(d)) leading to the horizontal polarized far field pattern with broadside radiation as can be seen from the Fig. 9 (g) and Fig. 9 (h).The induced modal surface current on the top located patch can also be found along the similar direction. The other excitable modes as mentioned in Fig. 8(c) either produce very high grating lobes or null at the broadside direction which can not be excited with the present feeding consideration and not shown in the present analysis.The aforementioned analysis justifies the fact that the presence of the leaky ring slot for the proposed ungrounded leaky wave antenna creates a leaky aperture mode away from its resonance. As a result of which, the grounded leaky wave antenna generates the top radiation only, essentially from the leakage of the periodically arranged patches. But for the proposed case, the ungrounded leaky discontinuity contributes its part and make the overall antenna radiate in both the hemisphere. The generation of the dual beam leaky radiation is common in literature and has earlier been realized based on mirrored and non-mirrored straight or interdigital slots for enhanced scanning range as can be seen in [5], [14], [15], [16], and [17]. The radiation discontinuity of these antennas can merely produce either omni-directional or bi-directional unit radiation pattern, leading to the overall bi-directional beam scanning in its single operating band including broadside. These antennas neither posses any frequency dependent unit radiation pattern with diverse radiation feature in two different operating bands nor feature any enhanced frequency sensitivity. Unlike them, the proposed leaky wave discontinuity uses patch and ring slot based resonator that can produce enhanced frequency sensitivity and induce two different and dis-similar unit radiation pattern at the two different operating band thereby making the antenna pattern-diverse and multi-functional leaky wave structure while scanning at its both the lower and upper operating band. To the best of the author's knowledge, this is the first time where a dual band leaky wave antenna is proposed exploiting the MMR concept which can provide fast forward and dual backward beam scanning feature.

III. ANTENNA DESIGN, SIMULATION, IMPLEMENTATION AND MEASUREMENT

In this section the overall leaky wave antenna is implemented and its' performance is simulated numerically and verified through measurement. Fig. 10 illustrates the final optimized

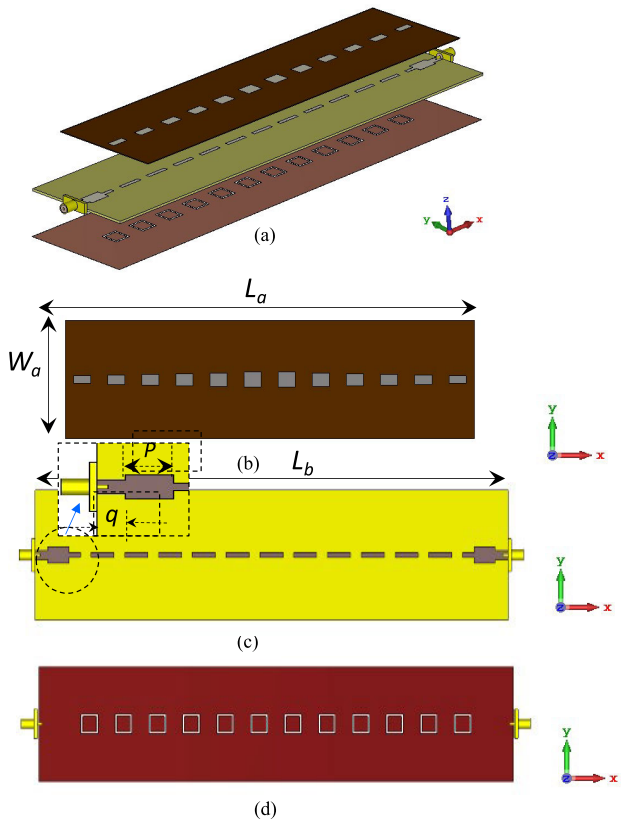

FIGURE 10. The final optimized antenna configuration (all dimension in mm): (a) Perspective view (b) Top layer: $L_a = 240$, $W_a = 60$ (c) Middle layer: $L_b = 280$, $W_a = 60$, $p = 12.5$, $q = 7.5$ (d) Bottom layer.

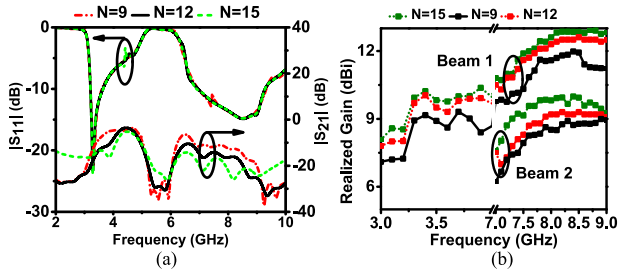

FIGURE 11. Variations in (a) S-Parameters and (b) Gain of the leaky wave antenna are investigated for the proposed design, considering different numbers of unit cells.

via-less leaky wave antenna configuration comprising 12 proposed unit cells arranged periodically along the X direction. The top rectangular patches are parasitically excited by a gap loaded microstrip line as depicted in Fig. 10(c). The width of the top patches has been modulated as described in the previous section to get radiation patterns with reduced side lobe levels at the upper band. The number of unit cells to be considered for the optimum performance of the leaky wave antenna is examined by analyzing the scattering and the far field responses of it. This is depicted in Fig. 11 (a) and 11 (b). It is evident that with 9 unit cells (N =9 the minimum no of unit cells considered in this experiment),

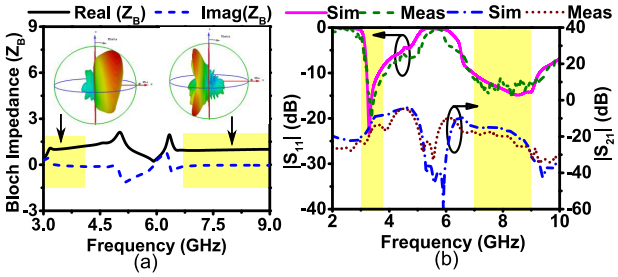

FIGURE 12. (a) Variation of Bloch impedance with frequency (b) Comparison of the simulated and measured S-parameters of the proposed antenna.

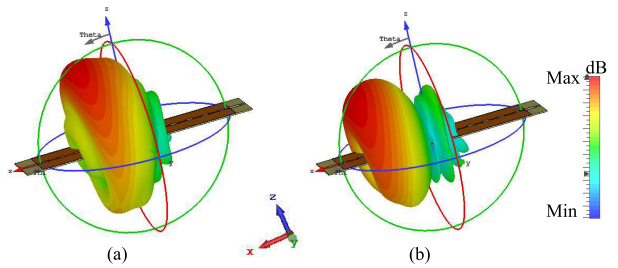

FIGURE 13. 3D Radiation pattern at lower band at two frequency scanned point (a) 3.2 GHz (b) 3.4 GHz.

a significant amount of power reaches the other port before contributing to radiation leakage as compared to the other cases of N = 12 and 15 at the upper band. This is reflected at the highest value of the transmission coefficient at the upper band in Fig. 11(a). However the transmission coefficient stays below −10 dB in this band for all the considered cases that is N = 9, 12 and 15. In the lower band the transmission coefficient shows similar variation for different no of the unit cells while maintaining the peak value at −7dB (for N = 9 unit cells i.e. for shortest LWA). The transmission coefficient of below −10 dB is observed to be a very good benchmark for good directional gain and radiation efficiency. The average radiation efficiencies at the lower band for N = 12 and 15 are noted to be around 85% to 90%. But, with the lowest number of unit cells (N = 9) the radiation efficiency is dropped below 80% causing a peak gain drop of more than 1.5 dBi at this band. At the upper band the differential gain improvement of less than 0.8 dBi is observed for Beam 1 (Bottom hemisphere beam) and no change in radiation efficiency is observed between the two cases of N = 12 and N = 15. This fact can be seen from the Fig.11(b). But with the lowest no of unit cells considered, the peak gain is observed 1 dB below at this band. Similar trend of variation in gain is followed for the Beam 2 (Upper hemisphere beam) as well at the same band. However, a difference of more than 2.5 dBi in gain value can be spotted between the two beams (Beam 1 and Beam 2) at the upper band. It is noted that even after increasing the number of unit cells to more than 15, the differential improvement in gain and efficiency is very less. On the other hand, increasing the number of

unit cells makes the antenna more bulky. Hence the prototype antenna is designed and simulated by combining 12 unit cells sequentially in the longitudinal direction ensuring that most of the accepted power radiates before it reaches the other end of the port while maintaining a compact profile. A feed section on either side is separately designed so that the antenna can be matched at its two frequency bands and shown in the zoomed portion of Fig. 10(c). Fig. 12(a) reports the normalized bloch impedance Z_B of the proposed structure, where

$$Z_B = \pm Z_0 \sqrt{\frac{(1+S_{11})^2 - S_{21}^2}{(1-S_{11})^2 - S_{21}^2}} \tag{10}$$

It can be seen that the real part of it is unity and the variation in the imaginary part is around 0Ω over both the bands. Hence, the structure can be easily matched to 50Ω for both the bands. Inset of the Fig. 12(a) shows the radiation behavior in each band. Fig 12(b) shows a good agreement between the reported simulated and measured reflection coefficient of the proposed LWA. The lower band is resonating between 3.2 GHz and 3.6 GHz while the upper band resonance is observed between 6.9 GHz and 9.1 GHz. Minor variations can be attributed as compared to the unit cell due to the loading of the feed and finite ground plane effect. The total length of the antenna is observed to be $5.6\lambda_0$ (at 6 GHz). Fig. 13 (a) and (b) shows the simulated 3D radiation pattern at two representative frequency points within the lower band namely 3.2 GHz and 3.4 GHz, respectively. In this band the antenna can be found to scan in the forward direction with increasing frequency. Also no radiation is observed in the bottom hemisphere. The bottom radiation is observed to be −18 dB down as compared to its forward co-polarized power. Simulated 3D radiation pattern at the upper band is also reported in Fig.14 for comparison. Three representative frequency pattern namely 7 GHz, 8 GHz and 9 GHz are chosen in Fig.14 (a), Fig.14 (c), Fig.14 (e), respectively, for this. In addition, Fig.14 shows the simulated magnitude of the electric field distribution of the antenna as well in the X-Z plane at the corresponding frequencies and are reported in Fig.14 (b), Fig.14 (d), Fig.14 (f). From these plots it can be inferred that the antenna at this band radiates in both the hemisphere and scans in the backward direction. The E-field distribution in the X-Z plane reveals the formation of the planar wave-fronts in both the upper and bottom hemisphere and shows the similar backward scan behavior as the frequency progresses. The hardware prototype of the proposed antenna and its mounting inside the anechoic chamber are illustrated in Fig. 15. Fig. 16 represents the comparison of the simulated and the measured radiation pattern in the XZ plane. From Fig. 16(a), it can be seen that the antenna scans in the forward direction between 12^0 and 57^0 as the frequency is swept from 3.2 GHz to 3.6 GHz. In the upper band, as the frequency is swept from 7 GHz to 9.2 GHz, the antenna radiates in the backward direction with two out-of-plane beams in its each frequency scanned points as can be seen in the Fig. 16(b). From this plot, it can

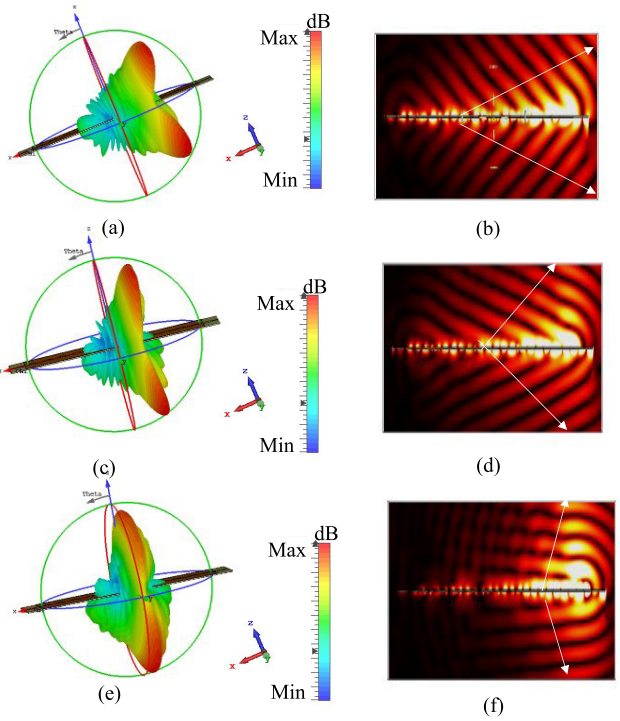

FIGURE 14. Simulated 3D radiation pattern and E-field distribution at X-Z plane at the upper band (a) Pattern at 7 GHz (b) E-Field at 7 GHz (c) Pattern at 8 GHz (d) E-Field at 8 GHz (e) Pattern at 9 GHz (f) E-Field at 9 GHz.

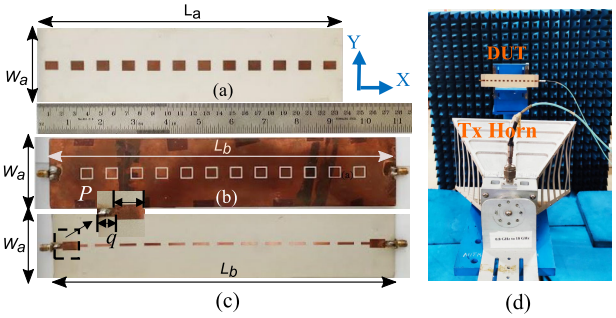

FIGURE 15. Fabricated antenna prototype and its mounting in anechoic chamber (a) Top Layer (b) Bottom Layer (c) Middle layer (d) antenna mounted in anechoic chamber.

be seen that, in the upper hemisphere, the simulated beam (named as beam 2) steers between -50^0 and -2^0, while in the lower hemisphere the simulated beam (named as beam 1) scans from -132^0 to -178^0 within the band of 7.0 GHz and 9.3 GHz. For the measured radiation patterns depicted in the same figure, beam 2 steers from -49^0 to -3^0, and beam 1 steers from -129^0 to -177^0 over the entire operating band in the same frequency scanned points, which agrees well with the simulated ones. The measured cross polarization level is below −40 dB, for both the bands. The average radiation efficiencies in lower and upper bands are calculated to be 75% and 92%, respectively shown in Fig. 17(a) and (b). Fig. 17 represents the simulated gain, the measured gain and the scan angle behavior of the proposed antenna for

TABLE 1. Comparison of proposed work with the current state-of-the-art.

Ref	Radiation Discontinuity	Broadside Radiation	Freq (GHz)	Scan Angle (Degree)	Gain Variation	Max X-pol (Meas) (dBi)	Scanning rate (Deg/ GHz)
[4]	SIW + Slot	Yes	(10.3 – 14.7), (14.7 – 16.3)	LB: (37^0 - 73^0), UB: (-70^0 - 0^0), (0^0 - 32^0)	(5, 5)	-30	(25^0, 16^0) **
[8]	Microstrip + Iris	No	(8.2 – 9.4), (13.2 15.2)	LB: (19^0 - 78^0), UB: (24^0 - 84^0)	(3.7, 3.6)	NA	(50^0, 30^0)
[9]	SIW + U slot	No	(5.25 - 6.25), (7.75 – 9)	(LB: (30^0 - 65^0), UB: (-46^0 - -10^0))	(3,2)	(-12.7, 7)	(15^0, 12^0)
[11]	SIW + Rectangular and Circular slot	No	(9 - 10.7), (13.4 – 16.2)	(LB: (107^0 - 167^0), UB: (-41^0 - -114^0))	(4,2)	(-5, -10)	(35^0, 24^0)
[12]	DMC + MSL	Yes (LB)	(5.8 - 8.5), (35 – 41.5)	(LB: (-64^0 - 0^0), UB: (11^0 - 70^0))	(8,8)	(NA, NA)	(23^0, 9^0)
[13]	Microstrip + Via	No	(5.8 – 6.9), (7.7 – 10.1)	LB: (-48^0 - -10^0), UB: (-56^0 - -6^0), (8^0 - 40^0))	(5, 3, 2.5) *	(-10, -10)	(34.5^0, 34.1^0)**
[14]	SIW + Slot	No	(9.6 - 11.2)	SB: 66^0	1.8	-20	66^0
[20]	SIW + Slot	No	(8.6 - 9.2), (10 - 12), (12.5 - 15.5)	LB: (42^0 - 71^0), UB1: (-40^0 - 4^0), UB2:(-55^0 - 54^0)	(6, 4, 3)	-20	(48.3, 22^0, 36.6^0)
[28]	Microstrip + Slot stub	No	(2.4 - 2.6)	(8^0 - 35^0)	NA	NA	135^0
[29]	Microstrip + CRLH	Yes	(5.95 - 7.1)	(-60^0 - 58^0)	2	-20	102^0
[30]	HMSIW + SPP TL	No	(8.65 - 9.5)	(-65^0 - -2^0) (-6^0 - 51^0)	1.5	NA	120^0**
[PW]	**Microstrip line + Ring slot+ Patch**	**No**	**(3.2 - 3.6), (6.9 - 9.1),**	**LB: (12^0 - 57^0), UB: (-49^0 - -3^0) - Beam 2 (-129^0 - -177^0) - Beam 1**	**(2,2,2) ***	**(-40,-40)**	**(112.5^0, 45^0) ****

PW: Proposed work, LB: Lower Band, UB: Upper Band *Dual beam gain variation in upper band, ** Total (sum) scanning rate for dual beam case

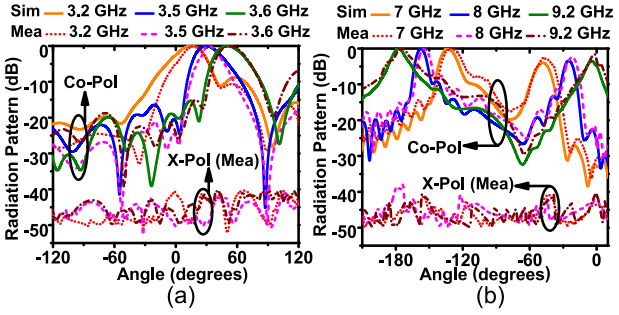

FIGURE 16. XZ plane radiation patterns (a) Lower band (b) Upper band.

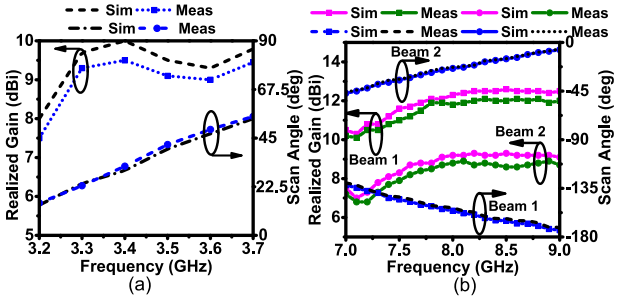

FIGURE 17. Variation of simulated and measured gain and scanning angle with frequency for (a) Lower band (b) Upper band.

comparison. In the lower band, the simulated antenna gain varies between 8 and 10 dBi while the measured gain varies between 7.5 dBi and 9.5 dBi. The antenna at this band scans around 45^0 in the 400 MHz bandwidth range confirming a fast beam scanning rate of 112.5^0/GHz. From Fig. 17(b), it can be observed that the measured gains of the beam 1 and 2 are between 10 to 12 dBi and 6 to 9 dBi, respectively at the upper band. The simulated and the measured scan angle also agrees well with each other over the upper operating band. The scanning rates of the individual beams (beam 1 and beam 2) are added to calculate the overall scanning rate at the upper band, and the value is found to be 40^0/GHz.

Table 1 compares the proposed LWA with some of the other reported LWA antennas in terms of its performance measure. The dual band LWAs reported in [8], [9], [11], and [12] do not posses the dual beam and enhanced frequency scanning feature. The works in [28], [29], and [30] provide fast scanning feature but their operation is restricted in single band only. The antennas in [4], [13], and [20] employs SIW as their fundamental guiding structure and possess multi-band and dual-beam features but cannot provide fast scanning rate. The presence of via/iris in their basic radiation discontinuity, brings additional complexity and increased cross polarization level [4], [13] in the elevation plane. Nevertheless, via/iris plays a major role in these antennas to achieve important functionalities. The proposed dual frequency microstrip based via-less MMR assisted periodic leaky wave antenna is very simple in structure and possesses very low cross

polarization level, stable radiation pattern, fast-forward and dual-backward beam scanning capability without requiring a complex feeding arrangement.

IV. CONCLUSION

In this paper, a gap loaded microstrip line serves as the host transmission line to feed the periodic patch radiators at the top and the ring slots etched at the bottom. This unique arrangement exploits the MMR behavior leading to the forward and backward harmonics which is responsible mainly for the dual band leaky wave action. Since at the upper band, the radiation from the bottom is achieved through an etched rectangular slot of the antenna, while mounting one should be careful that the bottom radiating aperture should not be hindered by other metallic objects or bounded mediums that can alter its radiation. In the lower operating frequency region, the antenna provide fast beam steering in the forward direction, while in its upper operating frequency band, it can scan symmetrically and simultaneously in both the lower and upper hemisphere in the backward direction.

ACKNOWLEDGMENT

The authors would like to acknowledge the High Performance Computing (HPC) Center, Indian Institute of Space Science and Technology (IIST), Thiruvananthapuram, for providing the workstations for simulation, Rogers Corporation for providing the PCB samples through University Sample Program and Dassault Systemes for providing the CST Studio suite to simulate the whole structure numerically.

REFERENCES

[1] D. R. Jackson, C. Caloz, and T. Itoh, "Leaky-wave antennas," *Proc. IEEE*, vol. 100, no. 7, pp. 2194–2206, Jul. 2012.

[2] Y.-L. Lyu, F.-Y. Meng, G.-H. Yang, P.-Y. Wang, Q. Wu, and K. Wu, "Periodic leaky-wave antenna based on complementary pair of radiation elements," *IEEE Trans. Antennas Propag.*, vol. 66, no. 9, pp. 4503–4515, Sep. 2018.

[3] D. Zheng and K. Wu, "Multifunctional leaky-wave antenna with tailored radiation and filtering characteristics based on flexible mode-control principle," *IEEE Open J. Antennas Propag.*, vol. 2, pp. 858–869, 2021.

[4] Z. Li, K. Liu, M. Zhao, J. Lin, Y. Wei, C. Tang, Y. Wu, M. Wang, C. Fan, H. Zheng, and E. Li, "SIW periodic leaky-wave antenna design for suppressing the stopband $\beta_0 p = \pi$ and open stopband by multimode resonator concept," *IEEE Antennas Wireless Propag. Lett.*, vol. 22, pp. 928–932, 2023.

[5] Y. Dong and T. Itoh, "Composite right/left-handed substrate integrated waveguide and half mode substrate integrated waveguide leaky-wave structures," *IEEE Trans. Antennas Propag.*, vol. 59, no. 3, pp. 767–775, Mar. 2011.

[6] S. Otto, Z. Chen, A. Al-Bassam, A. Rennings, K. Solbach, and C. Caloz, "Circular polarization of periodic leaky-wave antennas with axial asymmetry: Theoretical proof and experimental demonstration," *IEEE Trans. Antennas Propag.*, vol. 62, no. 4, pp. 1817–1829, Apr. 2014.

[7] J. Liu, "Periodic leaky-wave antennas based on microstrip-fed slot array with different profile modulations for suppressing open stopband and n = -2 space harmonic," *IEEE Trans. Antennas Propag.*, vol. 69, no. 11, pp. 7364–7376, Nov. 2021.

[8] D.-J. Wei, J. Li, J. Liu, G. Yang, and W. Zhang, "Dual-band substrate-integrated waveguide leaky-wave antenna with a simple feeding way," *IEEE Antennas Wireless Propag. Lett.*, vol. 18, pp. 591–595, 2019.

[9] D. K. Karmokar and K. P. Esselle, "Periodic U-slot-loaded dual-band half-width microstrip leaky-wave antennas for forward and backward beam scanning," *IEEE Trans. Antennas Propag.*, vol. 63, no. 12, pp. 5372–5381, Dec. 2015.

[10] K. Rudramuni, B. Majumder, and K. Kandasamy, "Dual-band dual-polarized leaky-wave structure with forward and backward beam scanning for circular polarization-flexible antenna application," *Microw. Opt. Technol. Lett.*, vol. 62, no. 5, pp. 2075–2084, 2020. [Online]. Available: https://onlinelibrary.wiley.com/doi/abs/10.1002/mop.32285

[11] Q. Zhang, Q. Zhang, H. Liu, and C. H. Chan, "Dual-band and dual-polarized leaky-wave antenna based on slotted SIW," *IEEE Antennas Wireless Propag. Lett.*, vol. 18, no. 3, pp. 507–511, Mar. 2019.

[12] Y. Li and J. Wang, "Dual-band leaky-wave antenna based on dual-mode composite microstrip line for microwave and millimeter-wave applications," *IEEE Trans. Antennas Propag.*, vol. 66, no. 4, pp. 1660–1668, Apr. 2018.

[13] K. Rudramuni, B. Majumder, P. K. T. Rajanna, K. Kandasamy, and Q. Zhang, "Dual-band asymmetric leaky-wave antennas for circular polarization and simultaneous dual beam scanning," *IEEE Trans. Antennas Propag.*, vol. 69, no. 4, pp. 1843–1852, Apr. 2021.

[14] A. Sarkar, A. Sharma, M. Adhikary, A. Biswas, and M. Akhtar, "Bi-directional siw leaky-wave antenna using TE20 mode for frequency beam scanning," *Electron. Lett.*, vol. 53, no. 15, pp. 1017–1019, 2017.

[15] A. Sarkar, A. Sharma, A. Biswas, and M. J. Akhtar, "Compact CRLH leaky-wave antenna using TE20-mode substrate-integrated waveguide for broad space radiation coverage," *IEEE Trans. Antennas Propag.*, vol. 68, no. 10, pp. 7202–7207, Oct. 2020.

[16] A. Sarkar, A. H. Naqvi, and S. Lim, "(40 to 65) GHz higher order mode microstrip-based dual band dual beam tunable leaky-wave antenna for millimeter wave applications," *IEEE Trans. Antennas Propag.*, vol. 68, no. 11, pp. 7255–7265, Nov. 2020.

[17] W.-H. Li, B. Wu, H.-R. Zu, T. Su, and Y.-F. Fan, "Design of leaky wave antenna with wide angle backfire to forward beam scanning based on generalized pattern synthesis," *IEEE Trans. Circuits Syst. II, Exp. Briefs*, vol. 70, no. 7, pp. 2625–2629, Jul. 2023.

[18] D. K. Karmokar, K. P. Esselle, and T. S. Bird, "Wideband microstrip leaky-wave antennas with two symmetrical side beams for simultaneous dual-beam scanning," *IEEE Trans. Antennas Propag.*, vol. 64, no. 4, pp. 1262–1269, Apr. 2016.

[19] Z. L. Ma and L. J. Jiang, "One-dimensional triple periodic dual-beam microstrip leaky-wave antenna," *IEEE Antennas Wireless Propag. Lett.*, vol. 14, pp. 390–393, 2015.

[20] Y. Geng, J. Wang, Z. Li, Y. Li, M. Chen, and Z. Zhang, "Dual-beam and triband SIW leaky-wave antenna with wide beam scanning range including broadside direction," *IEEE Access*, vol. 7, pp. 176361–176368, 2019.

[21] D. Zheng, Y.-L. Lyu, and K. Wu, "Transversely slotted SIW leaky-wave antenna featuring rapid beam-scanning for millimeter-wave applications," *IEEE Trans. Antennas Propag.*, vol. 68, no. 6, pp. 4172–4185, Jun. 2020.

[22] K.-L. Chan and S. Judah, "A beam scanning frequency modulated continuous wave radar," *IEEE Trans. Instrum. Meas.*, vol. 47, no. 5, pp. 1223–1227, Oct. 1998.

[23] D. L. Marks, J. Gollub, and D. R. Smith, "Spatially resolving antenna arrays using frequency diversity," *J. Opt. Soc. Amer. A, Opt. Image Sci.*, vol. 33, no. 5, pp. 899–912, May 2016. [Online]. Available: https://opg.optica.org/josaa/abstract.cfm?URI=josaa-33-5-899

[24] D. Ma, J. Zhong, S. Shen, A. Dubey, C. Zhang, Q. Zhang, and R. Murch, "Single-shot frequency-diverse near-field imaging using high-scanning-rate leaky-wave antenna," *IEEE Trans. Microw. Theory Techn.*, vol. 69, no. 7, pp. 3399–3412, Jul. 2021.

[25] S. G. I. Slomian, J. Sorocki, and K. Wincza, "Composite right/left-handed leaky-wave antenna with adjustable radiation bandwidth," *J. Electromagn. Waves Appl.*, vol. 30, no. 8, pp. 1054–1063, 2016.

[26] W. Menzel and A. Moebius, "Antenna concepts for millimeter-wave automotive radar sensors," *Proc. IEEE*, vol. 100, no. 7, pp. 2372–2379, Jul. 2012.

[27] D. Xie and L. Zhu, "Microstrip leaky-wave antennas with nonuniform periodical loading of shorting pins for enhanced frequency sensitivity," *IEEE Trans. Antennas Propag.*, vol. 66, no. 7, pp. 3337–3345, Jul. 2018.

[28] G. Zhang, Q. Zhang, S. Ge, Y. Chen, and R. D. Murch, "High scanning-rate leaky-wave antenna using complementary microstrip-slot stubs," *IEEE Trans. Antennas Propag.*, vol. 67, no. 5, pp. 2913–2922, May 2019.

[29] H. Jiang, K. Xu, Q. Zhang, Y. Yang, D. K. Karmokar, S. Chen, P. Zhao, G. Wang, and L. Peng, "Backward-to-forward wide-angle fast beam-scanning leaky-wave antenna with consistent gain," *IEEE Trans. Antennas Propag.*, vol. 69, no. 5, pp. 2987–2992, May 2021.

[30] Z. Peng, W. Yang, S. Shi, M. Jiang, J. Gao, and G. Zhai, "High scanning rate asymmetrical dual-beam leaky wave antenna using sinusoidally modulated reactance superposing surface," *IEEE Trans. Antennas Propag.*, vol. 70, no. 12, pp. 12258–12263, Dec. 2022.
[31] S. Ma, G.-H. Yang, D. Erni, F.-Y. Meng, L. Zhu, Q. Wu, and J.-H. Fu, "Liquid crystal leaky-wave antennas with dispersion sensitivity enhancement," *IEEE Trans. Compon., Packag., Manuf. Technol.*, vol. 7, no. 5, pp. 792–801, May 2017.
[32] L. Cui, W. Wu, and D.-G. Fang, "Printed frequency beam-scanning antenna with flat gain and low sidelobe levels," *IEEE Antennas Wireless Propag. Lett.*, vol. 12, pp. 292–295, 2013.
[33] C. Balanis, *Antenna Theory: Analysis and Design*. Hoboken, NJ, USA: Wiley, 2015. [Online]. Available: https://books.google.co.in/books?id=PTFcCwAAQBAJ
[34] R. Harrington and J. Mautz, "Theory of characteristic modes for conducting bodies," *IEEE Trans. Antennas Propag.*, vol. AP-19, no. 5, pp. 622–628, Sep. 1971.

BASUDEV MAJUMDER (Member, IEEE) received the Ph.D. degree in electrical engineering from Indian Institute of Technology (IIT) Bombay, Mumbai, India, in 2017. From August 2017 to December 2017, he was an Assistant Professor with the Birla Institute of Technology and Science, Pilani (BITS Pilani), Hyderabad Campus, India. In December 2017, he joined the Department of Avionics, Indian Institute of Space Science and Technology (IIST), Department of Space, Government of India, as an Assistant Professor, where he has been an Associate Professor, since July 2022. He has made scientific contributions to leaky wave antennas, metasurfaces, and high-impedance surfaces. His current research interests include the broader aspect of the RF and applied electromagnetics, microwave, and millimeter (mm) wave circuit design. He was a recipient of the 2017 INSPIRE Faculty Award from the Department of Science and Technology, Government of India.

SARATH SANKAR VINNAKOTA received the B.Tech. degree in electronics and communication engineering from Jawaharlal Nehru Technological University, Hyderabad, Telangana, India, in 2013, the M.Tech. degree in communication engineering from Vellore Institute of Technology, Vellore, Tamil Nadu, India, in 2015, and the Ph.D. degree from the Department of Electrical and Electronics Engineering, Birla Institute of Technology and Science, Pilani (BITS Pilani), Hyderabad Campus, India. His current research interests include rectenna designs for wireless energy harvesting and wireless power transfer, metasurface antennas, leaky wave antennas, and microwave circuit design.

MADHUSUDHAN GOUD RANGULA (Member, IEEE) received the B.Tech. degree in electronics and communication engineering from Jawaharlal Nehru Technological University Hyderabad, India, in 2007, and the M.Tech. degree in communication engineering from the NITK Surathkal, India, in 2011, where he is currently pursuing the Ph.D. degree in EM wave manipulation and control using metasurfaces. From June 2011 to December 2016, he was an Assistant Professor with Lovely Professional University, Punjab, India. From January 2017 to August 2021, he was an Assistant Professor with the Sreenidhi Institute of Science and Technology, Hyderabad. His research interests include transmissive/reflective metasurface design for beam focusing, beam tilting, OAM generation, and polarization conversion applications.

KRISHNAMOORTHY KANDASAMY (Senior Member, IEEE) received the B.E. degree in electronics and communication engineering from Bharathiar University, Coimbatore, India, in 2003, the M.E. degree in communication systems from the College of Engineering, Anna University, Chennai, India, in 2007, and the Ph.D. degree in electrical engineering from Indian Institute of Technology Bombay, Mumbai, India, in 2016. He is currently an Associate Professor with the Department of Electronics and Communication Engineering, NITK Surathkal, Surathkal, India. He has authored more than 37 articles in international journals and 47 in conference papers. His current research interests include metamaterials, antenna engineering, microwave-integrated circuits (MICs), and monolithic MICs.